ORIGINAL ARTICLE

C. M. Oldenburg
J. L. Lewicki

On leakage and seepage of CO_2 from geologic storage sites into surface water

C. M. Oldenburg (✉) · J. L. Lewicki
Earth Sciences Division 90-1116,
Ernest Orlando Lawrence Berkeley
National Laboratory, 1 Cyclotron Road,
Berkeley, CA 94720, USA
E-mail: cmoldenburg@lbl.gov
Tel.: +1-510-486-7419
Fax: +1-510-486-5686
E-mail: jllewicki@lbl.gov

Abstract Geologic carbon sequestration is the capture of anthropogenic carbon dioxide (CO_2) and its storage in deep geologic formations. The processes of CO_2 seepage into surface water after migration through water-saturated sediments are reviewed. Natural CO_2 and CH_4 fluxes are pervasive in surface-water environments and are good analogues to potential leakage and seepage of CO_2. Buoyancy-driven bubble rise in surface water reaches a maximum velocity of approximately 30 cm s^{-1}. CO_2 rise in saturated porous media tends to occur as channel flow rather than bubble flow. A comparison of ebullition versus dispersive gas transport for CO_2 and CH_4 shows that bubble flow will dominate over dispersion in surface water. Gaseous CO_2 solubility in variable-salinity waters decreases as pressure decreases leading to greater likelihood of ebullition and bubble flow in surface water as CO_2 migrates upward.

Keywords Ebullition · CO_2 storage · Leakage · Seepage · Bubble flow

Nomenclature

A	Empirical fit parameter	P_{CO_2}	Partial pressure of CO_2 (Pa, atm)
A_d	Additional mass	P_{st}	Surface tension pressure (N m^{-2})
C_M	Mass factor	P_z	Hydrostatic pressure (Pa, atm)
C	Concentration (mole fraction)	q_{B_i}	Bubble gas transfer rate of species i (mol cm^{-2}s^{-1})
d	Radius in Stoke's Law (m)		
d_p	Porous media particle diameter (m)	r	Bubble radius (m)
D	Diffusivity and dispersivity (m^2 s^{-1})	r_p	Characteristic length scale of pore (m)
E	Total ebullition rate (mol cm^{-2} s^{-1})	R'	Equivalent pore throat radius (m)
F_b	Buoyancy force (N)	R_b	Bubble radius (m)
F^D	Diffusive flux (mol cm^{-2} s^{-1})	T	Temperature (°C)
F^E	Bubble (ebullition) flux (mol cm^{-2} s^{-1})	u_b	Bubble velocity (m s^{-1})
F_d	Drag force (N)	v	Stoke's velocity (m s^{-1})
F_E	Fraction ebullition flux	V_B	Bubble velocity in surface water (m s^{-1})
g	Gravitational acceleration (m s^{-2})	z	Vertical coordinate (m)
H	Henry's Law coefficient (Pa)	μ_w	Water viscosity (kg m^{-1} s^{-1})
K	Henry's Law coefficient (mol cm^{-3} atm^{-1})	ρ_g	Gas-phase density (kg m^{-3})
k	Permeability (m^2)	ρ_f	Fluid density (kg m^{-3})
m	Mole flux (mol cm^{-2} s^{-1})	ρ_w	Water density (kg m^{-3})
n	Porosity	r	Surface tension (N m^{-1})
N_i	Molar content of gas species i (mol)	h	Contact angle (degrees)
P	Pressure (Pa, atm)	[ ]	Concentration (mol cm^{-3})

Introduction

Geologic carbon sequestration is the capture of anthropogenic CO_2 (e.g., from power-plant flue gases) and its storage in deep underground formations such as depleted oil and gas reservoirs and deep brine-filled formations. The purpose of geologic CO_2 storage is to reduce net atmospheric emissions of CO_2 to mitigate potential climate change associated with the role of CO_2 as a greenhouse gas. Key issues associated with geologic CO_2 storage relate to the integrity of the geological reservoir with respect to containment of CO_2 so that (1) the strategy serves the intended purpose of reducing net CO_2 emissions, and (2) CO_2 does not leak from the intended storage site and seep out of the ground with associated health, safety, and environmental (HSE) risks. Previous studies have modeled CO_2 migration in the vadose zone of on-shore environments (e.g., Oldenburg and Unger 2003, 2004). However, in off-shore environments such as the North Sea (Torp and Gale 2004) and in humid areas such as the Texas Gulf Coast (Hovorka et al. 2004), leaking CO_2 will likely encounter surface water (ocean, rivers, lakes, wetlands) prior to entering the atmosphere. Consequently, there is a need to investigate the processes of CO_2 seepage into surface water in order to fully understand migration processes and associated HSE risks. Key questions include (1) What are the physical processes relevant to CO_2 migration through sediments and overlying surface water either as bubbles or as a dissolved component in water? (2) Does surface water attenuate or enhance CO_2 seepage flux? (3) Under what conditions can CO_2 concentrations build up at depth and lead to the potential for catastrophic release?

These questions were investigated for the case where CO_2 seeps at relatively low fluxes into surface-water bodies. CO_2 migration through sediment pore water immediately below surface-water bodies in which liquid water is the primary connected phase and the CO_2 exists either in discrete bubbles or as a dissolved component in the aqueous phase was also considered. CO_2 in bubbles can be in gaseous, supercritical, and liquid phases over the range of possible surface- and pore-water systems relevant to CO_2 leakage and seepage. Results are presented here covering natural CO_2 and CH_4 fluxes, bubble rise in water and in saturated porous media, analysis of ebullition versus dispersive transport for CO_2 and CH_4 migrating into shallow water, and solubility of CO_2 in water at a wide range of depths and water compositions.

Definitions and environment

Terminology

Table 1 shows key terms and definitions that apply to gas migration and transport in surface water and subjacent

Table 1 Terminology related to gas migration

Term	Definition
Leakage	Migration in the subsurface away from the primary containment formation, e.g., through a fault or abandoned well.
Seepage	Migration across a boundary such as the ground surface or from subsurface rock or sediments into surface water.
Bubble	Immiscible volume of a secondary fluid phase (e.g., supercritical, gas, liquid) within a primary connected phase (e.g., aqueous).
Ebullition	Formation of bubbles from a liquid supersaturated with respect to dissolved gases, either in surface water or in groundwater.
Bubble flow	Flow of component(s) as transported in discrete bubbles.
Channel flow	Flow of component(s) as transported in a secondary connected fluid phase within a primary liquid phase.
Dissolution	Uptake of volatile components into solution in the liquid phase.
Advection	Component transport driven by movement of a phase containing the component.
Diffusion	Component transport driven by concentration gradients within a phase.
Dispersion	Component transport by small-scale advective motions and by diffusion that can be modeled collectively as a diffusive process.

saturated sediments. In general, low CO_2 fluxes and high CO_2 solubility in surface water favor dissolution and dispersive transport, while relatively high fluxes and low solubility of CO_2 favor ebullition and bubble flux. Bubble transport in surface water is familiar to everyone from observing the behavior of CO_2 bubbles in carbonated beverages. The flow of gases upward in porous media is not as familiar to people, although fluidized beds and packed-bed reactors with gas flow are well-known chemical processing techniques in which bubbles flow through porous media (Iliuta et al. 1999).

Environment of interest

The focus of this review is on CO_2 migration upward through saturated sediments and overlying surface water, including rivers, lakes, wetlands, estuaries, and continental shelf marine environments. Salinity, depth, temperature, and degree of mixing are all key characteristics that bear on the question of CO_2 transport. Non-specific leakage pathways upward from the deep CO_2 injection horizons may be capable of delivering CO_2 to the shallow environment. These leakage pathways could be along abandoned wells, faults or fault zones, but it is assumed that by the time the CO_2 reaches the shallow sediments below surface water, the CO_2 flux is relatively small. Large fluxes, e.g., from

well blowouts, will be obvious HSE risks that will be mitigated as quickly as possible. Of more concern from the HSE perspective are small fluxes that may be harder to detect (e.g., Oldenburg et al. 2003; Lewicki et al. 2005) but which could lead to HSE consequences, either in the long-term or due to near-surface buildup and rapid emission such as Lake Nyos (Sigurdsson et al. 1987).

Below surface water bodies, CO_2 can be in gaseous, supercritical, or liquid conditions. As shown in the phase diagram for pure CO_2 (Fig. 1), CO_2 has a critical point of 73.8 bars (7.38 Mpa) and 31.0°C, and is a gas at ambient atmospheric temperature and pressure (1 bar (0.1 Mpa), 25°C). The wide band on Fig. 1 indicates a P–T path within the earth assuming a geothermal gradient of 25°C km^{-1} and hydrostatic pressure and passes almost directly through the critical point. In continental onshore conditions studied in the past (Oldenburg and Unger 2003), the P–T path from depth to surface passes below the critical point. By such a path, CO_2 changes from supercritical to gaseous, and undergoes no large jumps in physical properties (e.g., density or viscosity) as it passes through 31°C at pressures below 73.8 bars. In contrast, in the offshore or deep surface-water condition, the P–T path will traverse part of the liquid-stability field from depth to the surface because of the hydrostatic pressure in the surface water and lack of geothermal gradient. In Fig. 1, the top edge of the wide band can be considered to be a sub-surface-water P–T path, and the bottom edge a sub-onshore P–T path. The transition from gaseous to liquid CO_2 or vice versa is associated with strong changes in density, viscosity, and solubility with implications for CO_2 seepage into surface water.
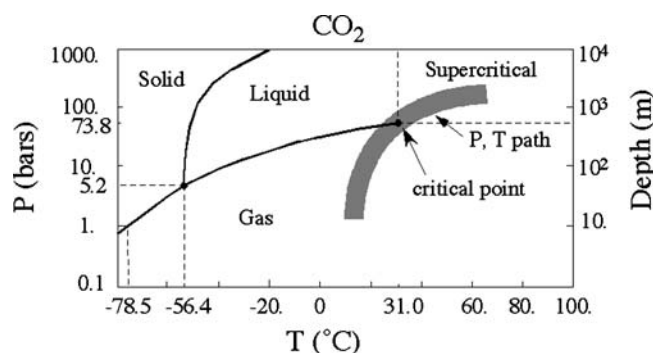

Fig. 1 Phase diagram for CO_2 showing typical P–T path with depth in the earth

Natural analogue CO_2 and CH_4 fluxes

Groundwater

Recent studies have quantified the flux of CO_2 derived from deep crustal and mantle origin that is dissolved and transported by shallow groundwaters (e.g., Evans et al. 2002; Chiodini et al. 1999, 2000). For example, throughout Tyrrhenian Central Italy, widespread non-volcanic CO_2 degassing occurs from vent and diffuse soil gas emissions and from CO_2-enriched groundwaters (Chiodini et al. 1999). From the Tyrrhenian Sea to the Apennine Mountains, buried structural highs act as gas traps from which gas may escape to the surface. Carbon dioxide is then released to the atmosphere either directly through gas emissions or by degassing from groundwater. Measured CO_2 partial pressure (P_{CO_2}) values for springs are up to four orders of magnitude greater than that of the atmosphere (Chiodini et al. 1999). Therefore, when groundwater is discharged at the surface, it releases a large amount of the carbon through CO_2 degassing. Chiodini et al. (1999, 2000) found that in geographic regions characterized by thick regional carbonate aquifers, most or part of the deeply derived gas is dissolved by the aquifers. In regions with smaller aquifers, extensive vent and soil CO_2 emissions occur at the surface because these smaller aquifers cannot dissolve all of the CO_2. Chiodini et al. (2000) estimated fluxes of deeply derived CO_2 up to 0.29 g m^{-2}d^{-1} into the carbonate Apennine aquifers.

Evans et al. (2002) conducted a chemical, isotopic, and hydrologic investigation of cold springs around Mammoth Mountain, California, USA. Based on these data, they estimated that the cold groundwater system around Mammoth Mountain discharges $\sim 2 \times 10^4$ tonnes y^{-1} of magmatic carbon (as CO_2), indicating that these waters have the ability to dissolve and transport large quantities of deeply derived CO_2. They also interpreted the 1×10^5 tonnes CO_2 y^{-1} that degasses diffusely through soils at Mammoth to be the gas that exceeds the dissolving capacity of the groundwater.

Shipton et al. (2004a, b) investigated the northern Paradox Basin (Utah, USA) as a natural analogue for CO_2 leakage. Here, CO_2 of deep-crustal origin migrates from numerous reservoirs (high P_{CO_2} shallow aquifers) along faults to the surface. An important loss of CO_2 to the atmosphere occurs as groundwaters discharge as springs at the surface and CO_2 degasses, as is evidenced by continual bubbling of CO_2 from many of these springs (Shipton et al. 2004a, b).

Wetlands

Much attention has focused on understanding the origin, transport, and fate of CH_4 in wetlands (e.g.,

Harriss and Sebacher 1981; Wilson et al. 1989; Mac-Donald et al. 1998; Walter and Heimann 2000; Rosenberry et al. 2003; Christensen et al. 2003) because these regions contain large quantities of stored organic carbon that, if released as CH_4, may strongly influence global climate. Although CH_4 differs from CO_2 in many ways, it is a reasonable proxy for CO_2 in terms of migration in surface water. Wilson et al. (1989) showed from repeated measurements of CH_4 flux in a temperate freshwater swamp, that this flux was highly variable over space and time. Ebullition from the bottom sediments was an important form of CH_4 release. Although ebullition was only recorded in 19% of their measurements, it accounted for 34% of the total flux over time. However, unlike many other studies, they found that flux was not correlated with water depth. Rosenberry et al. (2003) presented hydraulic-head data for a peatland in northern Minnesota, USA, which indicated that the peatland was overpressured at depth and the amount of overpressuring varied over time, with rapid declines likely caused by ebullition events. Christensen et al. (2003) measured in a closed laboratory system diffusion and ebullition fluxes of CH_4 from monoliths taken from wetland ecosystems in Sweden. They showed that ebullition accounts for 18 to 50% of the total CH_4 flux from their system and that this may represent a minimum contribution relative to that expected in nature due to stable laboratory conditions (e.g., isothermal, no wind).

Rivers

Smith et al. (2000) measured both diffusive and bubbling CH_4 fluxes in open water, bare soils, macrophyte mats, and flooded forest along the Orinoco River floodplain, Venezuela. They found that due to productivity, the flooded forest environment accounted for the highest diffusive and bubble fluxes and that ebullition accounted for 65% of all emissions. Large temporal variations in CH_4 fluxes were also observed due primarily to seasonally fluctuating water levels, with ebullition higher during dry seasons. Where the Little Grand Wash Fault Zone crosses the Green River (Utah, USA), CO_2 of deep-crustal origin discharges into the Green River. Here, a line of gas bubbles is observed along the fault trace (e.g., Shipton et al. 2004a, b).

Lakes and reservoirs

In non-volcanic lake environments, CO_2 and CH_4 are primarily derived from biologic processes. The primary pathways of gas exchange between water and the atmosphere are molecular diffusion across the air–water interface and bubble flow through the water column. Pathways of exchange of CO_2 and CH_4 between the lake and the atmosphere differ significantly because of contrasts in CO_2 and CH_4 aqueous solubility, and concentrations in the epilimnion and in the atmosphere. Because the solubility of CH_4 in water is about an order of magnitude less than that of CO_2 (1 bar, 20°C), elevated CH_4 concentrations at depth lead to ebullition, whereas elevated aqueous CO_2 concentrations can build up at depth. Many lakes are supersaturated with respect to CO_2, particularly in the wintertime, when productivity and therefore photosynthetic uptake is low. Ebullition is the primary release mechanism of CH_4 from lakes and other shallow water environments. However, bubbling is episodic and dependent on a variety of factors such as temperature, water depth, barometric pressure variations, winds, and related bottom shear stress (e.g., Keller and Stallard 1994; Walter and Heimann 2000; Rosenberry et al. 2003; Joyce and Jewell 2003). Casper et al. (2000) found that based on measured CO_2 and CH_4 concentration gradients with depth in a small freshwater lake in the UK, ebullition accounted for 96% of the CH_4 flux and diffusion accounted for 99% of the CO_2 flux. The rate of gas ebullition was highly variable in space and time and decreased with water depth.

The transport and fate of CO_2 in lakes in volcanic environments have been of great interest due to the lethal gas bursts that occurred at Lakes Monoun and Nyos, Cameroon, in 1984 and 1986, respectively. Approximately 1,800 people were killed in these combined events by the hypothesized rapid overturn and depressurization of CO_2-rich lake waters (derived from emission of magmatic CO_2 into the lakes) and subsequent large-scale CO_2 ebullition. These lakes displayed density stratification and within the deep anoxic stagnant layers, P_{CO_2} built up to equal the ambient hydrostatic pressure (Sigurdsson et al. 1987; Oskarsson 1990; Giggenbach 1990). The rapid lake overturn may have been driven by precipitation, landslides, or wind-driven mixing. The resultant ebullition led to the gas bursts at the surface (Sigurdsson et al. 1987; Oskarsson 1990; Giggenbach 1990). In the Lake Nyos event, 240,000 tonnes of CO_2 were lost from the upper 100 m of the lake (Giggenbach 1990). Giggenbach et al. (1991) showed that other CO_2-rich lakes worldwide (Laacher See, Germany, Dieng, Indonesia, and Mt. Gambier, Australia) display similar chemical and physical characteristics to Lakes Nyos and Monoun. In general, seasonal overturn, other periodic deep mixing processes, or man-made degassing schemes (e.g., Halbwachs et al. 2004) are needed to prevent density stratification and the potential for extreme buildup of CO_2 at depth in lakes subject to CO_2 influxes at depth.

Marine environments

Hovland et al. (1993) presented a review of CH_4 degassing from shallow marine sediments worldwide and estimated the global flux. They showed that CH_4 occurs at aqueous saturation concentrations and in free gas form at many locations in the upper layers of marine sedimentary basins. This CH_4 originates either from microbial degradation of organic material in shallow sediments or at greater depth in sedimentary basins by thermal ''cracking'' of organic materials to form petroleum hydrocarbons. In many locations, CH_4 escapes from shallow marine sediments to the water column as continuous or intermittent bubble flow. For example, in the Gulf of Mexico, gas seeps are associated with different geological environments such as deltaic sediments, salt domes, and gas hydrates in sediments on and at the base of the continental slope (Anderson and Bryant 1990). In the Tommeliten field of the North Sea, gas migrates along deep-seated faults and evidence of gas close to the seabed is present over an area of $\sim$120,000 m^2 (Hovland and Judd 1988). Gas seeps accounting for $\sim$120 bubble streams are predominantly found within 6,500 m^2 of this area. At Cape Lookout Bight, a marine basin on the Outer Banks of North Carolina, USA, shallow sediment pore waters become saturated with CH_4 during the summer and ebullition occurs during low tide due to reduction in hydrostatic pressure (Martens and Klump 1980). Martens and Klump (1980) estimated that $\sim$15% of the CH_4 in the bubbles here dissolves during transit through the water column and $\sim$6.9$\times$10^7 g CH_4 y^{-1} are lost to the atmosphere.

The area off the coast of Santa Barbara, California, perhaps the most well studied and quantified hydrocarbon seep field in the world, shows extensive bubbling gas plumes seeping from faults and fractures along the axes of anticlinal hydrocarbon traps (e.g., Hornafius et al. 1999; Leifer et al. 2000; Washburn et al. 2001; Boles et al. 2001). Based on sonar data, Hornafius et al. (1999) estimated that the total emission rate of hydrocarbons into the water column through ebullition was $1.7 \pm 0.3\times10^5$ m^3 d^{-1} (18 km^2 area). Leifer et al. (2000) investigated shallow (< 70 m) seeps and found that near-surface aqueous CH_4 concentrations were $> 10^8$ times atmospheric equilibrium values. The fraction of gas that is released to the atmosphere versus dissolved in the water column depends both on the seep and the surface-water properties. Boles et al. (2001) monitored gas bubble flow rates from a large seep (67 m depth) where gas is captured by two steel tents and piped to shore to be processed. They observed that tidal forcing caused bubble flow rate to vary by 40% around the average flow rate and high and low tides were correlated with reduced and increased flow rates, respectively.

CO_2 leakage and bubble flow

Bubble formation fundamentals

For a bubble to form and persist in water, the pressure within the bubble must be greater than the ambient hydrostatic pressure plus the surface tension of water that must be overcome to form the bubble. Mathematically, the pressure inside the bubble (P) is equal to the sum of the partial pressures of the volatile species which must be in excess of the sum of the ambient hydrostatic pressure at depth z (P_z) and the surface tension pressure (P_{st}):

$$P = \sum_i C_i H_i > P_z + P_{st} \qquad (1)$$

where H_i are the Henry's law coefficients (Pa or atm) for each species i, C_i are the aqueous concentrations of the volatile species (mole fractions), and the fluid pressure at depth z is given by

$$P_z = P_A + \rho_w g z \qquad (2)$$

where ρ_w is water density, g is gravity, and P_A is atmospheric pressure. The P_{st} in Eq. 1 is related to the bubble radius (r) and the surface tension (σ) of the water according to the Young–Laplace equation (e.g., Pellicer et al. 2000) as

$$P_{st} = \frac{2\sigma}{r} = P - P_z. \qquad (3)$$

Surface tension for water is approximately 72 dynes cm^{-1} (0.072 N m^{-1}), which means that P_{st} is negligible relative to P_z for bubbles with radius larger than approximately 150 μm (0.15 mm) for which $2\sigma/r \sim$ 0.1 bar (e.g., Leifer and Patro 2002).

The surface tension pressure (P_{st}) implies that the gas pressure in the bubble must be higher than the gas saturation pressure in the ambient aqueous phase. The bubble gas-phase composition is determined by the relative magnitude of the gas partial pressures and thus reflects the volatility (the inverse of the component's aqueous-phase solubility) of each species and the water composition. This relationship of ebullition to solubility is a key factor in CO_2 leakage because waters with varying solubility due to different salinity, pressure, and temperature may be encountered during the long rise upward of CO_2 bubbles.

Once a bubble is formed and rises upwards, it can exchange mass with the surrounding water. The bubble molar flux to surrounding water, F_i, is expressed as:

$$F_i = \frac{dN_i}{dt} = q_{B_i} 4\pi r^2 \left(C_i - \frac{P_{B_i}}{H_i} \right), \qquad (4)$$

(e.g., Leifer and Patro 2002) where N_i is the molar content of gas species i in the bubble, q_{B_i} is the individual

bubble gas transfer rate, and P_{B_i} is the bubble gas partial pressure.

Equation 4 is applied to each gas species in the bubble individually. Because the gas flux is driven by the difference $C_i - P_{B_i}/H_i$, gas outflows from the bubble when $C_i > P_{B_i}/H_i$ and inflows when $C_i > P_{B_i}/H_i$ (e.g., Leifer et al. 2000). In the case of a bubble composed predominantly of CO_2, it will dissolve as CO_2 outflows and grow as dissolved air (primarily N_2 and O_2) and/or CO_2 inflow. If for example, C_{CO_2} is elevated due to bubble dissolution, the gas outflow from the bubble is decreased. If concentrations of dissolved O_2 and N_2 in the water column are low, inflow will be reduced and dissolution will occur. With rise through the water column, CO_2 may dissolve and the bubble may shrink, increasing P_{st} as the bubble radius decreases (see Eq. 3). Also, bubble expansion will occur due to decreasing P_z and associated gas expansion. Upon rising and increasing in size, the larger bubble will be able to transfer gas more efficiently because of the increased surface area. The total gas entering the water column from rising bubbles depends on the cumulative integrated bubble molar flux over the lifetime of the bubbles.

For applications involving CO_2 rising from the deep subsurface due to leakage from geologic CO_2 storage sites, the CO_2 can be in either a supercritical or liquid phase as well as a gas phase (see Fig. 1). The above fundamentals apply also for these cases in which the bubble contains immiscible supercritical or liquid phase CO_2.

Steady-state bubble rise in surface water

Assuming that the bubble persists throughout its rise through the surface-water body, the bubble lifetime can be derived from the water-body depth divided by the bubble rise velocity. The velocity of bubble rise is often given by Stoke's law:

$$v = d^2 g \left(\frac{\rho_w - \rho_g}{18\mu_w} \right) \tag{5}$$

where d is bubble diameter, ρ_w and ρ_g are water and gas density, respectively, and μ_w is water viscosity. By this well-known equation, the bubble velocity is directly related to the square of bubble diameter. Therefore, as P_z decreases, d increases and bubbles accelerate. However, Eq. 5 is only valid at very small Reynolds number ($Re = \rho_w v d/\mu_w < \sim 1$) corresponding to either very small bubble size, small buoyancy contrast, or a very viscous liquid. For CO_2 bubbles in surface water, Re is of order 1 when bubble diameter is of order 10^{-4} m (0.1 mm). In summary, Eq. 5 is a poor predictor of gas bubble rise velocity in surface water, except for very small bubbles.

A wealth of empirical data from experiments and field measurements has provided a sound basis for estimating bubble rise velocity for larger bubbles. Leifer and Patro (2002) showed data from experiments of bubble rise velocity as a function of bubble radius, with contours of Reynolds number (dashed lines) (Fig. 2). Equation 5 applies only in the lowermost left-hand corner at $Re < 1$, and furthermore the rate of bubble rise in water has a maximum of approximately 30 cm s^{-1} which is reached when the bubble diameter is approximately 1.5 mm ($r = 0.75$ mm). Bubbles are known to begin oscillating and become non-spherical at radii of approximately 0.7 mm and Re of 400, leading to a decrease in rise velocity as bubble radius increases. While these results are valid strictly for air bubbles, very similar results would be obtained for pure CO_2 gas bubbles, since the driving force is given by the difference in density between the gas phase and water, a negligible difference when comparing the buoyancy of air ($\rho = 1.2$ kg m^{-3}) to gaseous CO_2 ($\rho = 1.8$ kg m^{-3}) for bubbles in water ($\rho = 1,000$ kg m^{-3}) at near-surface conditions.

Bubble and channel flow

Within a water-saturated porous medium such as the sediments or fractured rock below a surface-water body, upward buoyancy forces will act on CO_2 bubbles. However, within porous media, bubble flow is restricted by the presence of solid matrix grains and the tortuous path around them. In addition, capillary forces can arise from (1) contact of the bubble with the solid grains, and (2) the deformation of the bubble and corresponding
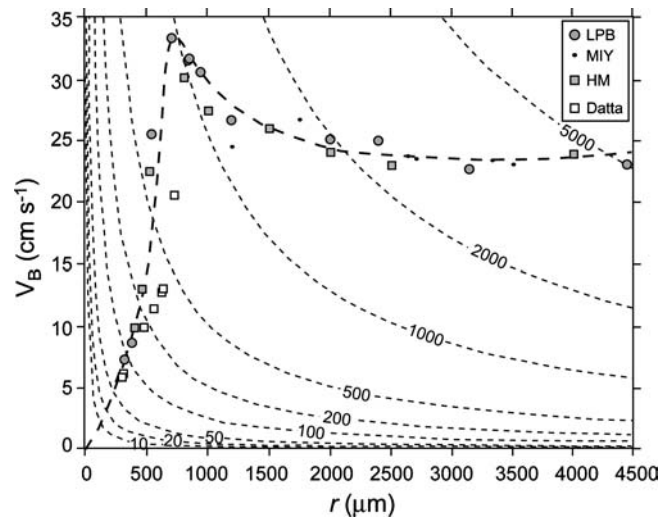

Fig. 2 Bubble rise velocity as a function of bubble radius with background contours of Reynolds number (from Leifer and Patro 2002)

change in bubble radius (r) (see Eq. 3) that occur when the bubble squeezes through narrow pore throats. Pore throats can also lead to straining and trapping processes that block bubble flow (e.g., Wan et al. 2001). Bubble rise in porous media is therefore significantly more complicated than bubble rise in standing surface water.

Figure 3 is a sketch of two different end-members for gas flow in porous media: (1) discrete bubbles, and (2) channel flow. If the gas flux is low, gases can migrate upward through pore bodies and throats as small individual bubbles, with deformation and blockage occurring as controlled by solid matrix grains (Fig. 3a). In contrast, when the flux is large, gas bubbles can be larger and/or more numerous leading to greater entrapment and coalescence. When entrapment and coalescence exceed a threshold, a connected channel of gas forms between the leading edge of water displacement and the gas source. When this connectivity occurs, gas flow can be driven by gas-pressure-gradient rather than buoyancy forces, and these pressure-gradient forces can overcome the capillary, permeability, and/or liquid displacement resistances and displace water. Flow in a channelized regime is further favored by the low gas viscosity.

The additional complexity of capillary forces due to the solid matrix grains can be quantified by reference to the Bond number (Bo), the ratio of buoyancy forces driving upward flow to surface tension forces that tend to retard bubble flow. The Bond number can be defined as

$$Bo = \frac{\left(\rho_{\mathrm{w}} - \rho_{\mathrm{g}}\right) g\, r_{\mathrm{p}}^2}{\sigma} \qquad (6)$$

(e.g., Brooks et al. 1999) where r_{p} is a characteristic length scale of the pore space. When $Bo > 1$, buoyancy forces dominate, and when $Bo < 1$, capillary forces dominate. Considering values of ρ_{w}, ρ_{g}, g, and σ of 1,000 kg m^{-3}, 1.8 kg m^{-3}, 9.81 m s^{-2}, and 7.2×10^{-2} N m^{-1}, respectively, capillary forces will dominate for pore sizes less than approximately 3 mm. Capillarity will therefore be the important force in medium and fine-grained porous media. A modified Bo can be defined to include pore body and pore throat length scales to account for the fact that buoyancy is more important in pore bodies, while capillarity is more important in pore throats (Brooks et al. 1999).

The Bo can be used to classify whether gas flow in saturated porous media will occur by bubble or channel flow (Brooks et al. 1999). Bubble flow occurs when buoyancy forces dominate and gravity drives gas bubbles upward without large capillarity effects. Such flow will occur when the porous media are coarse, such as in gravels and coarse sands. In contrast, fine porous media give rise to stronger capillary forces as gas is squeezed through small pore throats leading to gas becoming trapped by capillarity. As trapped gases accumulate in the medium, eventually they may form connected paths to the gas source area and pressure-driving forces can be propagated from the source to the gas–liquid front. If snap-off occurs isolating the leading gas-phase region from the gas source, capillarity can again stop the rise of the gas bubble. In this way, the rise of gas in medium and fine-grained porous media typically occurs only by channel flow (Fig. 3). This has been observed in experimental studies of upward air flows in the field of air sparging for remediation of volatile contaminants (e.g., Ji et al. 1993). Beyond the theoretical considerations of Bo, formation heterogeneity inherent in the subsurface can also control channel formation.

Steady-state bubble rise in porous media

Recent studies (Roosevelt and Corapcioglu 1998; Corapcioglu et al. 2004) motivated by the need to understand air movement in air sparging are useful for CO_2 migration also. The methods of Corapcioglu et al. (2004) were used to predict CO_2 bubble rise velocity in porous media for both gaseous and liquid CO_2. This analysis is valid only for single-bubble rise in coarse sediments, i.e., $Bo > 1$.

The analysis begins by considering the forces of buoyancy, drag, and surface tension acting on a single

Fig. 3 Schematic of flow regimes in porous media: (**a**) bubble flow, and (**b**) channel flow
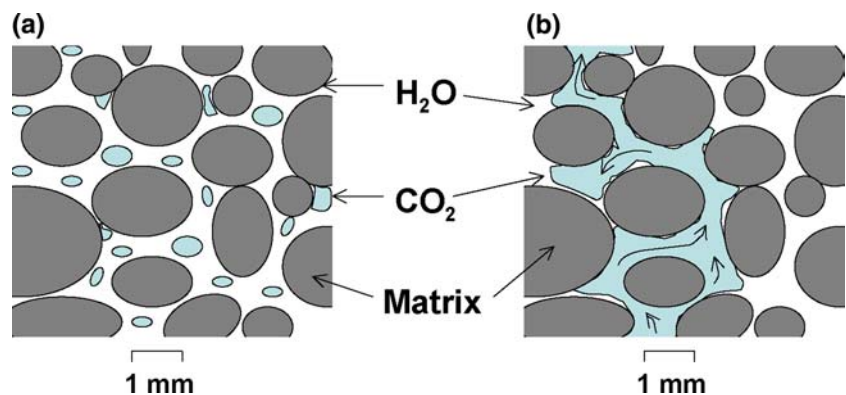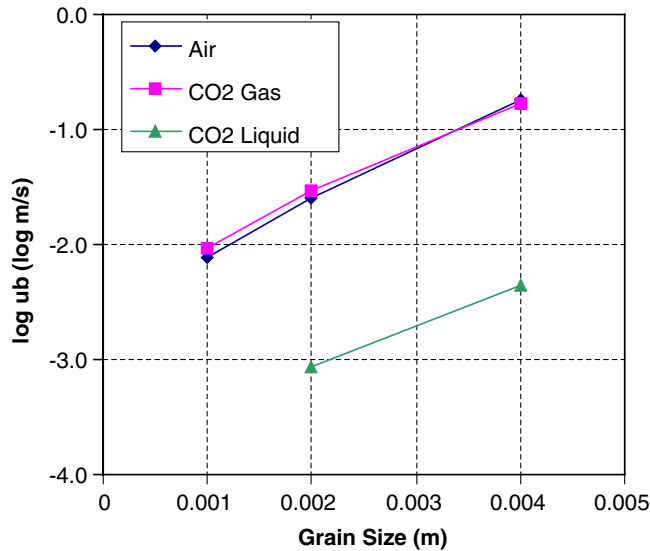
Fig. 4 $\log_{10} u_b$ for three different coarse porous media as a function of particle size

bubble in a porous medium. For a bubble rising at steady-state, the upward buoyancy forces are exactly balanced by the surface tension and drag forces that tend to retard motion. The force balance equations of Corapcioglu et al. (2004) are presented in Appendix A, while values for various terms are given in Table 2. Many assumptions are made in the analysis, such as constant contact angle, bubble radius, and fit parameter (Corapcioglu et al. 2004).

Bubble-rise velocities were calculated for the 4 mm glass beads of Corapcioglu et al. (2004) and two slightly finer grain sizes where d_p = 2 and 1 mm (Table 3). The approach breaks down for medium and fine grain sizes as evidenced by the negative rise velocity produced as a

Table 2 Fluid properties for the analysis of bubble flow in porous media

Property	Symbol	Value	Units
Surface tension	σ	7.2×10^{-2}	N m^{-1}
Contact angle	Q	30	degrees
Viscosity of water	μ_w	1×10^{-3}	kg m^{-1} s^{-1}
Density of water	ρ_w	1,000	kg m^{-3}
Viscosity of air	μ_g	1.80×10^{-5}	kg m^{-1} s^{-1}
Density of air	ρ_g	1.2	kg m^{-3}
Viscosity of CO_2			
Gas (1 bar, 20°C)	μ_g	1.47×10^{-5}	kg m^{-1} s^{-1}
Liquid (61 bars, 22°C)	μ_l	6.33×10^{-5}	kg m^{-1} s^{-1}
Density of CO_2			
Gas (1 bar, 20°C)	ρ_g	1.8	kg m^{-3}
Liquid (61 bars, 22°C)	ρ_g	755.2	kg m^{-3}
Gravitational acceleration	G	9.81	m s^{-2}
Additional mass	A_d	1	–
Fit parameter	A	26.8	–

Table 3 Porous media properties and results for bubble flow in porous media

Property	Symbol	Units	4 mm glass beads[a]	Gravelly sand[b]	Coarse sand[b]
Porosity	n	–	0.3954	0.3	0.35
Particle size	d_p	m	4×10^{-3}	2×10^{-3}	1×10^{-3}
Bubble radius	R_b	m	4×10^{-3}	2×10^{-3}	1×10^{-3}
Equivalent pore throat radius	R'	m	3.09×10^{-4}	1.55×10^{-4}	7.73×10^{-5}
Rise velocity					
Air	u_b	m s^{-1}	1.83×10^{-1}	2.52×10^{-2}	7.73×10^{-3}
CO_2 gas	u_b	m s^{-1}	1.68×10^{-1}	2.91×10^{-2}	9.40×10^{-3}
CO_2 liquid	u_b	m s^{-1}	4.43×10^{-3}	8.60×10^{-4}	N/A
Burke–Plummer permeability	k	m^2	1.80×10^{-8}	1.47×10^{-9}	6.76×10^{-10}

[a] Corapcioglu et al. (2004)
[b] de Marsily (1986)

solution to the quadratic equation (Eq. A.12). Results are shown in Fig. 5. The logarithm of the calculated bubble-rise velocities for three coarse grain sizes (d_p = 4, 2, and 1 mm) for air and CO_2 gas bubbles, along with the calculated rise velocity for a CO_2 liquid bubble, are plotted. The maximum velocity is approximately 18 cm s^{-1}, which is considered by Corapcioglu et al. (2004) to be the maximum possible porous media bubble rise velocity. For the 4 mm grain size, the CO_2 bubble is predicted to rise slightly slower than the air bubble, but CO_2 bubbles are predicted to rise slightly faster than air bubbles for the less-coarse media. This cross-over effect appears to be due to the greater buoyancy of air relative to CO_2 and its importance in coarse media, and the
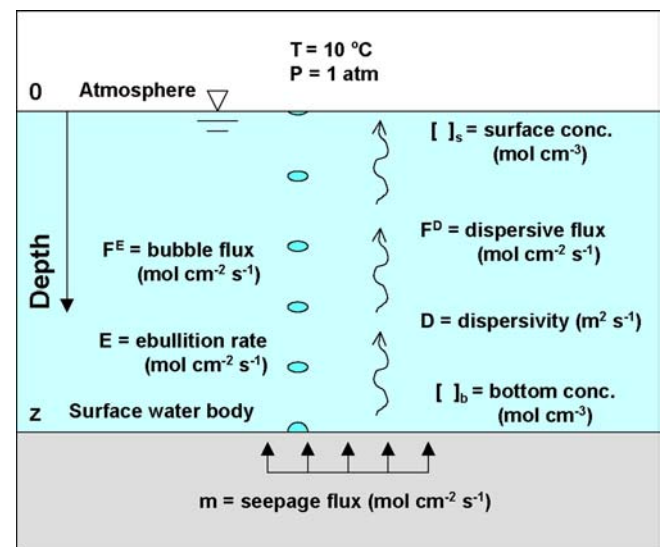

Fig. 5 Schematic of domain and variables for ebullition versus dispersive mass transport analysis. Ebullition is indicated by the bubbles, dispersion by the wiggly vector

greater importance of the lower viscosity of CO_2 relative to air in finer media. Finally, CO_2 liquid bubbles rise more slowly due to their greater density and viscosity than CO_2 gas bubbles. Despite the numerous simplifying assumptions in this analysis, the calculations reveal the importance of grain size, and density and viscosity contrast in predicting bubble rise velocity in coarse porous media. As for medium and fine porous media, gas flow will be by channel flow which can be analyzed by a wide range of multiphase reservoir simulation methods.

Transport by bubble flow and diffusion in surface water

To examine ebullition and diffusion rate, a surface-water system consisting of air (N_2 and O_2), CO_2, and CH_4 similar to that described by Morel and Herring (1993) was used. If seepage of CO_2 and/or CH_4 occurs across the sediment surface at depth z into the overlying surface water body at a constant flux m (mol cm^{-2} s^{-1}), the rates of ebullition and diffusion of these species can be estimated (Fig. 5). The following assumptions are made: (1) bubble formation maintains the sum of the partial pressures (CO_2, CH_4, air, H_2O) at P_z, i.e., P_{st} is neglected, (2) bubbles rise so fast through the water column to the surface that no dissolution occurs, (3) transport of all solutes in the water column is described by a dispersion coefficient ($D = 10^{-3}$ cm^2 s^{-1}), and (4) chemical reactions (e.g., bicarbonate formation from CO_2, oxidation of CH_4) are ignored. The equations governing ebullition rate and steady-state mass balance from which estimates of diffusive flux (F^D) and ebullition flux (F^E) of CO_2 and CH_4 for given seepage fluxes (m) can be calculated are presented in Appendix B.

F^D and F^E were calculated for three cases: (1) seepage of CO_2 and CH_4 into a surface water body where m_{CO_2} = m_{CH_4}, (2) seepage of CO_2 only, and (3) seepage of CH_4 only. In each case (Cases 1–3), a water body with z = 50, 1,000, and 10,000 cm, low, medium, and high m_{CO_2} and/or m_{CH_4} values, respectively, was considered (Table 4 shows Henry's Law coefficients and Table 5

shows m_{CO_2} and m_{CH_4} values), and percent ebullition of total flux for the species that seep into the water body calculated. The low, medium, and high fluxes used correspond approximately to the low, medium, and high seepage fluxes calculated in prior vadose-zone-related work (Oldenburg and Unger 2003, 2004). For comparison, natural fluxes of CO_2 from plant and soil biological processes are approximately 10^{-9} mol cm^{-2} s^{-1} (10 μmol m^{-2} s^{-1}) efflux to 3×10^{-9} mol cm^{-2} s^{-1} (30 μmol m^{-2} s^{-1}) uptake (e.g., Baldocchi and Wilson 2001).

The results (Table 5) show that diffusion is important for transport of CO_2 to the atmosphere in water bodies up to 1,000 cm deep and for m_{CO_2} up to the medium values considered. At greater m_{CO_2} or z, CO_2 is transported to the atmosphere almost entirely by ebullition. For CH_4, diffusion is only an important transport mechanism for shallow (50 cm) water bodies and low m_{CH_4}, accounting for about half the total CH_4 flux. For cases where CH_4 seeps into deeper water bodies of (z = 1,000 and 10,000 cm) or m_{CH_4} is elevated, ebullition accounts almost entirely for the CH_4 flux to the atmosphere. These differences between ebullition and diffusion fluxes for CO_2 and CH_4 are due to the greater solubility of CO_2 in water relative to CH_4.

Table 5 Percentage of flux by ebullition relative to diffusion for various depths and flux proportions

Case	z (cm)	m^{CO_2} (mol cm^{-2} s^{-1})	m^{CH_4} (mol cm^{-2} s^{-1})	% $F^E_{CO_2}$	% $F^E_{CH_4}$
1	50	4.59×10^{-11}	4.59×10^{-11}	4	49
1	1,000	4.59×10^{-11}	4.59×10^{-11}	31	92
1	10,000	4.59×10^{-11}	4.59×10^{-11}	45	95
1	50	4.59×10^{-10}	4.59×10^{-10}	32	92
1	1,000	4.59×10^{-10}	4.59×10^{-10}	82	99
1	10,000	4.59×10^{-10}	4.59×10^{-10}	89	100
1	50	4.59×10^{-9}	4.59×10^{-9}	82	99
1	1,000	4.59×10^{-9}	4.59×10^{-9}	98	100
1	10,000	4.59×10^{-9}	4.59×10^{-9}	99	100
2	50	9.18×10^{-11}	0	8	NA
2	1,000	9.18×10^{-11}	0	49	NA
2	10,000	9.18×10^{-11}	0	63	NA
2	50	9.18×10^{-10}	0	31	NA
2	1,000	9.18×10^{-10}	0	90	NA
2	10,000	9.18×10^{-10}	0	94	NA
2	50	9.18×10^{-9}	0	90	NA
2	1,000	9.18×10^{-9}	0	99	NA
2	10,000	9.18×10^{-9}	0	99	NA
3	50	0	9.18×10^{-11}	NA	68
3	1,000	0	9.18×10^{-11}	NA	96
3	10,000	0	9.18×10^{-11}	NA	98
3	50	0	9.18×10^{-10}	NA	96
3	1,000	0	9.18×10^{-10}	NA	100
3	10,000	0	9.18×10^{-10}	NA	100
3	50	0	9.18×10^{-9}	NA	100
3	1,000	0	9.18×10^{-9}	NA	100
3	10,000	0	9.18×10^{-9}	NA	100

Table 4 Henry's law coefficients (K_i) for different P_z values (Spycher, unpublished code)

z (m)	P_z(atm)	K_{CO_2}(mol atm^{-1} cm^{-3})	K_{CH_4}(mol atm^{-1} cm^{-3})	K_{air}(mol atm^{-1} cm^{-3})
Surface-50 cm	1	4.90×10^{-5}	1.98×10^{-6}	1.29×10^{-6}
1,000	2	4.87×10^{-5}	1.98×10^{-6}	1.29×10^{-6}
10,000	11	4.63×10^{-5}	1.92×10^{-6}	1.26×10^{-6}

K values are for 10°C
K_{air} is the average of K_{N_2} and K_{O_2}

## Transport of dissolved CO₂ in surface water

Transport of the dissolved fraction of CO_2 in surface water will occur by diffusive and dispersive processes. Flow occurs in typical surface waters such as rivers, lakes, estuaries, and shallow seas by combinations of gravity, wind, and tidal forcings (e.g., Fischer et al. 1979). Such motions are often turbulent and involve a wide range of chaotic flow velocities over a range of length scales which lead to effective dispersion and mixing of dissolved species. Dispersion and mixing will periodically expose surface water to the atmosphere, where it will potentially equilibrate with atmospheric CO_2 creating an effective outgassing that is equal to the bottom seepage flux at steady state. In lakes, mixing may be somewhat less than in rivers or coastal environments. Vertical mixing may occur only once or twice a year, or in some special cases not at all, for example, in deep equatorial lakes, or lakes with permanent ice cover (Goldman and Horne 1983). In addition, the density of CO_2-saturated water is approximately 1% greater than that of pure water (Ennis-King and Paterson 2003), creating the possibility of dissolved CO_2 producing a stable density stratification. However, in typical surface waters, flow forcings such as gravity, wind, and tides will dominate over density stratification and cause mixing on time scales much smaller than the carbon sequestration time scale (hundreds to thousands of years). Thus rivers, lakes, estuaries, and continental shelf ocean water will not be effective at attenuating leakage and seepage fluxes of CO_2 occurring as a dissolved component. Furthermore, ebullition will generally occur for the flux magnitudes of interest thus subordinating the importance of diffusion and dispersion to the overall bubble transport of CO_2 seepage in surface water.

Effects of pressure, temperature, and salinity on ebullition

As shown by the differences in ebullition flux between CO_2 and CH_4, the solubility of gas species is a fundamental control on ebullition. The solubility of CO_2 is a strong function of salinity, pressure, and temperature, all of which may vary within the subsurface and surface waters. CO_2 solubility for various H_2O–NaCl mixtures was calculated using the methods of Spycher and Pruess (2004) and Spycher et al. (2003). The case of a 200-m deep surface-water body at 10°C and underlying porous media with a geothermal gradient equal to 30°C km⁻¹ and hydrostatic pressure assuming $\rho_{H_2O} = 1,000$ kg m⁻³ was considered. The various solubility profiles are plotted as a function of depth in Fig. 6. The two curves on the left-hand side of Fig. 6 are for a hypersaline brine and a typical oilfield brine and are plotted only up to the sediment–water interface because they are normally found in the subsurface. The other two curves are those of seawater and freshwater and are continuous from subsurface into surface water. The CO_2 density profile is calculated from the online NIST Webbook (Lemmon et al. 2003) for pure CO_2 at the given pressures and temperatures.

The first point to note in Fig. 6 is that CO_2 transitions from supercritical to liquid and then to gas as it rises upwards in this system. This is in stark contrast to the simple change from supercritical to gas (Fig. 1) that occurs in the absence of surface water (Oldenburg and Unger 2003). The implication of these phase transitions is that buoyancy forces on CO_2 bubbles are nearly constant with a slight decrease as the bubble rises, for example from −1,000 to −380 m. Then upon rising through the liquid–gas transition, the enormous density change in CO_2 will lead to approximately a factor of 3.7

Fig. 6 Solubility of CO_2 (mole fraction) in various brines assuming fully ionized salt as a function of depth within a surface-water body (0–200 m) and the underlying formation (−1,000 to 0 m) with the different phase stability fields for CO_2 indicated by the shading. *Right-hand side figures* show corresponding temperature, pressure, and density of CO_2 with depth
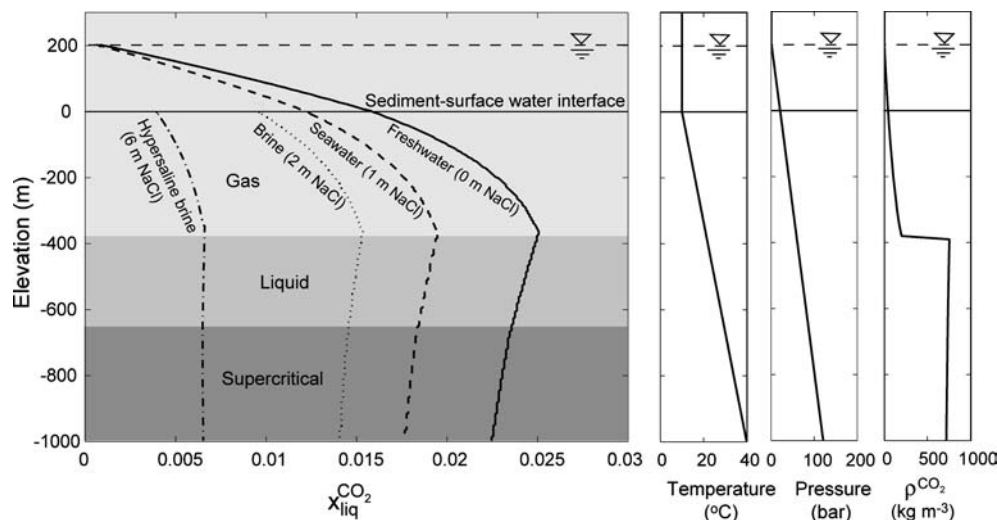
change in volume of the bubble, assuming an isothermal transition, with corresponding increase in upward buoyancy force.

The second important point illustrated in Fig. 6 is the variation in CO_2 solubility upward from depth. At intermediate and low salinity, CO_2 solubility rises slightly along a bubble migration path upward from depth until the liquid–gas transition point (depth equal to −380 m). From this point upward, CO_2 solubility declines rapidly as the pressure falls. The implication of this pattern for bubble transport is that CO_2 ebullition is favored as dissolved CO_2 is transported upwards from depths shallower than approximately −380 m in this system.

Finally, Fig. 6 shows dramatically the variation in solubility as a function of salinity of water. This has important implications for situations where the migration pathway of CO_2 leakage and seepage can traverse formations and surface water with contrasting salinity. For example, consider first the case of a briny groundwater system at depth with overlying fresher aquifers below a freshwater lake. In this case, a rising CO_2 bubble would encounter water with progressively higher CO_2 solubility, making it likely that CO_2 bubbles would disappear as the CO_2 dissolved into the aqueous phase. In contrast, there could be a system with fresh-water aquifers at depth underlying a shallow continental shelf marine environment. In this case, ebullition may become more important as salinity increases and pressure decreases as the CO_2 moves upwards. Combinations of the above transitions are of course possible. Figure 6 provides a general guide as to the trend toward greater dissolution or greater ebullition in water as a function of depth and salinity.

Summary

Numerous investigations have been conducted to measure natural CO_2 and CH_4 fluxes and concentrations in surface-water environments and to estimate the relative contributions of ebullition and dispersion to the total fluxes of these species to the atmosphere. These previous studies provide direct evidence of how CO_2 leakage and seepage fluxes of similar magnitude will behave, and they indicate that local conditions strongly control transport processes. Natural CO_2 and CH_4 fluxes and local concentrations are significant and can lead to ebullition making it challenging to discern low-flux leakage and seepage from natural emissions.

Prior studies of volcanic lakes that have undergone lethal CO_2 outgassing indicate that deep and stagnant conditions are conducive to the formation of waters that are supersaturated with respect to CO_2. Seasonal overturn, or other regular mixing processes such as natural convection by hydrothermal heating, neither of which occur at Lakes Nyos or Monoun, may prevent extreme buildup of CO_2 and associated potentially lethal outgassing events.

Previous work in the areas of bubble physics and hydrostatics indicate that for a bubble to form, the sum of the partial pressures of the volatile components must exceed the local hydrostatic pressure and surface tension. Once a bubble forms and rises upwards, mass transfer occurs between the bubble and liquid.

Although Stokes Law is not formally applicable to gas-bubble rise in surface water for bubble sizes larger than approximately 0.1 mm, empirical data exist to predict bubble rise velocity over a wide range of bubble sizes. Bubble-rise velocity reaches a maximum of approximately 30 cm s^{-1} for bubbles approximately 0.7 mm in radius and declines for larger bubbles due to turbulence and related bubble oscillations.

In saturated porous media, e.g., below surface water, small CO_2 fluxes can be sustained by bubble flow, especially in coarse and highly permeable porous media. For larger CO_2 fluxes, or finer porous media, transport is by channel flow.

Bubble-rise velocity in porous media has a maximum of approximately 18 cm s^{-1} in very coarse gravels. Bubble-rise velocity is much smaller in typical sediments, which can only sustain a small bubble flux of CO_2 before transitioning to channel flow. CO_2 rise velocity in the channel-flow regime is governed by multiphase flow processes that can be studied using reservoir engineering simulation approaches.

Bubble-rise velocity for a liquid CO_2 bubble is slower than for a CO_2 gas bubble due to the much smaller density contrast between liquid CO_2 and water than between gaseous CO_2 and water.

For the range of seepage fluxes and surface-water depths considered in this study, CO_2 transport through the surface water will tend to be by ebullition/bubble flux for relatively high seepage fluxes and/or deep water bodies and by diffusion/dispersion for relatively low seepage fluxes and/or shallow water bodies. Species such as CH_4 with lower solubility in water are more likely to be transported by bubble flux.

As leaking CO_2 rises upwards, liquid-stable CO_2 phase conditions may be encountered, especially if there is overlying surface water. Therefore, CO_2 rising from depth will transition from supercritical to liquid and then to gas with an upward rise. The transition from supercritical to liquid is not associated with a significant change in physical properties (e.g., density, viscosity, solubility), while the transition from liquid to gas has large changes in properties and these changes favor bubble flow.

The solubility of CO_2 in water depends strongly on the P, T, and salinity conditions of water and the phase properties of the CO_2. Leaking CO_2 rising from depth through saturated porous media of varying salinity may

tend to dissolve and/or undergo ebullition depending on the conditions. In general, CO_2 solubility decreases with depth at shallow depths, creating greater potential for ebullition as CO_2 rises upward into the near-surface environment.

Discussion

The results of this study allow the following comments on the key questions.

1. What are the physical processes relevant to the migration through sediments and overlying surface water of CO_2 either as bubbles or as a dissolved component in water? Bubbles are subject to buoyancy and surface tension forces in porous media, with surface tension dominating for fine porous media. CO_2 transport is likely to be by channel flow in the fine sediments below a surface-water body. These channels can be produced by bubble trapping and coalescence processes that arise in medium- and fine-grained porous media. Channels can also be created by the heterogeneity inherent in subsurface formations. Upon approaching the surface-water body as a second phase (gas or liquid) CO_2 bubbles will emanate from the sediment and rapidly rise upwards. Under this scenario, there is no ebullition process since the CO_2 already exists as a second phase in the porous media. Ebullition at the interface of sediment and surface water and/or dispersive transport of CO_2 seepage from the sediment interface will only occur for seepage fluxes on the order of the background flux or smaller. For larger fluxes, channel flow and bubble flow are expected in the porous media and in the surface water, respectively. Dissolved CO_2 in surface water is transported by motions of the aqueous phase and is typically driven by gravity, wind, and tidal forcings.
2. Does surface water attenuate or enhance CO_2 seepage flux? Rising CO_2 bubbles are subject to mass transfer with surrounding waters, but the travel times are relatively short because rise velocities are high. In general, CO_2 bubbles, once formed, are expected to rise from the bottom to the top of typical surface-water bodies as solubility decreases with decreasing pressure. As for dispersion of dissolved CO_2, mixing times in surface waters are short relative to geologic CO_2 sequestration times, and dissolved CO_2 added by leakage and seepage is expected to exsolve rapidly from surface water as it mixes and equilibrates with atmospheric CO_2. Thus CO_2 seepage flux is not expected to be significantly attenuated by surface water.
3. Under what conditions can CO_2 concentrations build up at depth and lead to the potential for catastrophic release? Water becomes slightly denser when it contains dissolved CO_2. Lakes with deep stagnant regions subject to CO_2 fluxes from below are prone to stratification with water at depth that is supersaturated with CO_2 and subject to rapid outgassing if there is a disturbance to the lake that initiates overturn. Natural mixing processes such as seasonal overturn and wind-driven mixing—largely absent from the equatorial Lakes Nyos and Monoun—and man-made degassing schemes can be effective at preventing CO_2 buildup in deep stagnant lakes.

Appendix A

Equations for bubble rise in porous media from Corapcioglu et al. ([2004](#)). The equations governing bubble rise in coarse porous media are derived by balancing forces due to buoyancy given by

$$F_b = \left(\rho_f - \rho_g\right) g \frac{4}{3} \pi R_b^3, \tag{7}$$

the surface tension force given by

$$F_{st} = 2\pi R' \sigma \sin\theta, \tag{8}$$

where R' is an equivalent pore throat radius, and the drag force given by

$$F_d = A \left[\frac{150\,\mu_b u_b (1-n)^2}{d_p^2\, n^3} + \frac{1.75\rho_g u_b^2 (1-n)}{d_p\, n^3}\right] \frac{4}{3}\pi R_b^3 \tag{9}$$

(variables are defined in Nomenclature). The first term in brackets in Eq. 9 is the Kozeny term, accounting for viscous drag in laminar flow, while the second term is the Burke–Plummer term, accounting for turbulent losses. Summing these three forces and allowing for acceleration of the bubble, we have the balance relation

$$F_b - F_d - F_{st} = A_d\, \rho_g \frac{4}{3}\pi R_b^3 \left(\frac{\partial u_b}{\partial t} + u_b \frac{\partial u_b}{\partial x}\right) \tag{10}$$

where the A_d term accounts for entrained liquid ahead of the bubble and is defined as

$$A_d = 1 + C_M \frac{\rho_f}{\rho_g} \tag{11}$$

Substituting the individual force equations and grouping terms by the powers of bubble rise velocity (u_b), we obtain

$$-\left(C_1 u_b^2 + C_2 u_b + C_3\right) = \frac{\partial u_b}{\partial t} + u_b \frac{\partial u_b}{\partial x} \tag{12}$$

where

$$C_1 = \frac{1.75\,(1-n)A}{d_p\,n^3\,A_d} \tag{13}$$

$$C_2 = \frac{150\,(1-n)^2 A\,\mu_b}{d_p^2\,n^3\,\rho_g\,A_d} \tag{14}$$

$$C_3 = \frac{1}{\rho_g\,A_d}\left[\frac{3}{2}\frac{R'\sigma\,\sin\theta}{R_b^3} - \left(\rho_f - \rho_g\right)g\right]. \tag{15}$$

The rise velocity (u_b) can be calculated using the coefficients of Eqs. 13–15 in the quadratic equation (12) for which we assume steady state and zero inertia, i.e., right-hand side of Eq. 12 is set to zero.

Appendix B

Equations for ebullition and diffusion rates are given from Morel and Herring (1993). For each species, the rate of ebullition E_i (mol cm^{-2} s^{-1}) is proportional to its partial pressure at the sediment surface:

$$E_i = \frac{P_i}{P_z}E \tag{16}$$

where E is the total rate of ebullition of all species together. A steady-state mass balance equation is written for each species at the sediment surface where the sum of its transport by diffusion and ebullition is equal to its rate of formation at depth:

$$\frac{D}{z}\left([CO_2]_b - [CO_2]_s\right) + EK_{CO_2}^{-1}[CO_2]_b P_z^{-1} = m, \tag{17}$$

$$\frac{D}{z}\left([CH_4]_b - [CH_4]_s\right) + EK_{CH4}^{-1}[CH_4]_b P_z^{-1} = m, \tag{18}$$

$$\frac{D}{z}\left([air]_b - [air]_s\right) + \frac{E[air]_b}{K_{air}P_z} = 0 \tag{19}$$

where the subscripts b and s refer to the bottom and surface concentrations (mol cm^{-3}), respectively, and K_i is the Henry's law constant for each gas species (mol cm^{-3}atm^{-1}), and the bottom air flux is assumed to be

zero. The diffusive flux is assumed to be driven by the concentration gradient across the entire depth of the surface-water body.

The aqueous concentrations of species at the surface are calculated to be in equilibrium with the atmosphere at 10°C, where $P_{CO_2}^{atm}$, P_{air}^{atm}, and $P_{CH_4}^{atm}$ are 3.12×10^{-4}, 1.97×10^{-6}, and 9.87×10^{-1} atm, respectively (see Table 4 for K_i values):

$$[CO_2]_s = P_{CO_2}^{atm}K_{CO_2} \tag{20}$$

$$[CH_4]_s = P_{CH_4}^{atm}K_{CH_4} \tag{21}$$

$$[air]_s = P_{air}^{atm}K_{air}. \tag{22}$$

Unknowns in the mass balance equations are now bottom concentrations and E, while the pressure condition at the sediment surface is:

$$P_{air} + P_{CH_4} + P_{CO_2} + P_{H_2O} = P_z. \tag{23}$$

P_{H_2O} in Eq. 23 can be neglected relative to the other volatile components and substitute Henry's law expressions to obtain

$$\frac{[CO_2]_b}{K_{CO_2}} + \frac{[CH_4]_b}{K_{CH_4}} + \frac{[air]_b}{K_{air}} = P_z \tag{24}$$

where K_i values are for the P_z considered (Table 4). With the approximations $[CO_2]_s << [CO_2]_b$ and $[CH_4]_s << [CH_4]_b$, bottom concentrations from Eqs. 17–19 are substituted into Eq. 24 to yield:

$$\frac{m}{K_{CO_2}D/z + E/P_z} + \frac{m}{K_{CH_4}D/z + E/P_z} + \frac{(D/z)[air]_s}{K_{air}D/z + E/P_z} = P_z. \tag{25}$$

By neglecting the first term in Eq. 25 and replacing K_{CH_4} and K_{air} with an average K value, an approximate solution for E can be obtained:

$$E = m + \left(\frac{D}{z}\right)[air]_s - \frac{P_z\,KD}{z} \tag{26}$$

Substitution of Eq. 26 into Eqs. 17 –19 gives the bottom concentrations of species:

$$[CO_2]_b \cong \frac{m}{D/z + EK_{CO_2}^{-1}P_z^{-1}} \tag{27}$$

$$[CH_4]_b \cong \frac{m}{D/z + EK_{CH_4}^{-1}P_z^{-1}} \tag{28}$$

$$[air]_b \cong \frac{(D/z)[air]_s}{D/z + EK_{air}^{-1}P_z^{-1}} \tag{29}$$

The diffusive and ebullition fluxes, F^{D} and F^{E}, respectively, of CO_2 and CH_4 can then be calculated:

$$F_{CO_2}^{\mathrm{D}} = \frac{D}{z}\left([CO_2]_b - [CO_2]_s\right) \quad (30)$$

$$F_{CH_4}^{\mathrm{D}} = \frac{D}{z}\left([CH_4]_b - [CH_4]_s\right) \quad (31)$$

$$F_{CO_2}^{\mathrm{E}} = EK_{CO_2}^{-1}[CO_2]_b P_z^{-1} \quad (32)$$

$$F_{CH_4}^{\mathrm{E}} = EK_{CH_4}^{-1}[CH_4]_b P_z^{-1} \quad (33)$$

References

Anderson AL, Bryant WR (1990) Gassy sediment occurrence and properties: northern Gulf of Mexico. Geo-Marine Lett 10:209–220

Baldocchi DD, Wilson KB (2001) Modeling CO_2 and water vapor exchange of a temperate broadleaved forest across hourly to decadal time scales. Ecol Modell 142:155–184

Boles JR, Clark JF, Leifer I, Washburn L (2001) Temporal variation in natural methane seep rate due to tides, Coal Oil Point area, California. J Geophys Res 106:27077–27086

Brooks MC, Zise WR, Annable MD (1999) Fundamental changes in in-situ air-sparging flow patterns. Ground Water Monit Rem 19(2):105–113

Casper P, Maberly SC, Hall GH, Finlay BJ (2000) Fluxes of methane and carbon dioxide from a small productive lake to the atmosphere. Biogeochemistry 49:1–19

Chiodini G, Frondini F, Kerrick DM, Rogie J, Parello F, Peruzzi L, Zanzari AR (1999) Quantification of deep CO_2 fluxes from Central Italy. Examples of carbon balance for regional aquifers and of soil diffuse degassing. Chem Geol 159:205–222

Chiodini G, Frondini F, Cardellini C, Parello F, Peruzzi L (2000) Rate of diffuse carbon dioxide Earth degassing estimated from carbon balance of regional aquifers: The case of the central Apennine, Italy. J Geophys Res 105:8423–8424

Christensen TR, Panikov N, Mastepanov M, Joabsson A, Stewart A, Oquist M, Sommerkorn M, Reynaud S, Svensson B (2003) Biotic controls on CO_2 and CH_4 exchange in wetlands–a closed environment study. Biogeochem 64:337–354

Corapcioglu MY, Cihan A, Drazenovic M (2004) Rise velocity of an air bubble in porous media: Theoretical studies. Water Resour Res 40:W04214. DOI 10.1029/2003WR002618

Ennis-King J, Paterson L (2003) Rate of dissolution due to convective mixing in the underground storage of carbon dioxide. In: Gale J, Kaya Y (eds) Proceedings of the 6th international conference on greenhouse gas control technologies, vol 1. pp 507–510

Evans WC, Sorey ML, Cook AC, Kennedy BM, Shuster DL, Colvard EM, White LD, Huebner MA. (2002) Tracing and quantifying magmatic carbon discharge in cold groundwaters: lessons learned from Mammoth Mountain, USA. J Volcanol Geotherm Res 114:291–312

Fischer HB, List EJ, Imberger J, Brooks NH (1979) Mixing in Inland and Coastal Waters. Academic Press, New York

Giggenbach WF (1990) Water and gas chemistry of Lake Nyos and its bearing on the eruptive process. J Volcanol Geotherm Res 42:337–362

Giggenbach WF, Sano Y, Schmincke HU (1991) CO2-rich gases from Lakes Nyos and Monoun, Cameroon; Laacher See, Germany, Dieng, Indonesia, and Mt. Gambier, Australia - variations on a common theme. J Volcanol Geotherm Res 45:311–323

Goldman CR, Horne AJ (1983) Limnology. McGraw-Hill, New York

Halbwachs M, Sabroux J-C, Grangeon J, Kayser G, Tochon-Danguy J-C, Felix A, Beard J-C, Veilleveille A, Vitter G, Rishon P, Wuest A, Hell J (2004) Degassing the "killer lakes" Nyos and Monoun, Cameroon. Trans Am Geophys Union EOS 85(3):281–285

Harriss RC, Sebacher D (1981) Methane flux in forested freshwater swamps of the southeastern United States. Geophys Res Lett 8:1002–1004

Hornafius SJ, Quigley D, Luyendyk BP (1999) The world's most spectacular marine hydrocarbon seeps (Coal Oil Point, Santa Barbara Channel, California): Quantification of emissions. J Geophys Res 104:20703–20711

Hovland M, Judd AG (1988) Seabed pockmarks and seepages: impact on geology, biology, and the marine environment. Graham & Trotman, London

Hovland M, Judd AG, Burke RA Jr (1993) The global flux of methane from shallow marine sediments. Chemosphere 26:559–578

Hovorka SD, Doughty C, Benson SM, Pruess K, Knox PR (2004) Assessment of the impact of geological heterogeneity on CO_2 storage in brine formations: a case study from the Texas Gulf Coast. In: Baines SJ, Gale J, Worden RH (eds) Geological storage of carbon dioxide for emissions reduction: technology, vol 233. Geological Society of London Special Publication, pp 147–163

Iliuta I, Ortiz-Arroyo A, Larachi F, Grandjean BPA, Wild G (1999) Hydrodynamics and mass transfer in trickle-bed reactors: an overview. Chem Eng Sci 54(21):5329–5337

Ji W, Dahmani A, Ahlfied DP, Lin JD, Hill E III (1993) Laboratory study of air sparging: Air flow visualization, Ground Water Monit Rem 13(4):115–126

Joyce J, Jewell PW (2003) Physical controls on methane ebullition from reservoirs and lakes. Env Eng Geosc 9:167–178

Keller M, Stallard RF (1994) Methane emission by bubbling from Gatun Lake, Panama. J Geophys Res 99:8307–8319

Leifer I, Patro RK (2002) The bubble mechanism for methane transport from the shallow sea bed to the surface: A review and sensitivity study. Continental Shelf Res 22:2409–2428

Leifer I, Clark JF, Chen RF (2000) Modifications of the local environment by natural marine hydrocarbon seeps. Geophys Res Lett 27:3711–3714

Lemmon EW, McLinden MO, Friend DG (2003) Thermophysical properties of fluid systems. In: Linstrom PJ, Mallard WG (eds) NIST Chemistry WebBook, NIST Standard Reference Database Number 69, National Institute of Standards and Technology, Gaithersburg, Maryland (http://www.webbook.nist.gov)

Lewicki JL, Hilley GE, Oldenburg CM (2005) An improved strategy to detect CO_2 leakage for verification of geologic carbon sequestration. Geophys Res Lett. 32(19):L19403. DOI 10.1029/2005GL024281

Macdonald JA, Fowler D, Hargreaves KJ, Skiba U, Leith ID, Murray MB (1998) Methane emission rates from a northern wetland—response to temperature, water table and transport. Atmos Environ 32:3219–3227

de Marsily G (1986) Quantitative hydrogeology. Academic Press, New York

Martens CS, Klump JV (1980) Biogeochemical cycling in an organic rich coastal marine basin. 1. Methane sediment-water exchange processes. Geochim Cosmochim Acta 44:471–490

Morel FMM, Hering JG (1993) Principles and applications of aquatic geochemistry. Wiley, New York

Oldenburg CM, Unger AJA (2003) On leakage and seepage from geologic carbon sequestration sites: unsaturated zone attenuation. Vadose Zone J 2:287–296

Oldenburg CM, Unger AJA (2004) Coupled vadose zone and atmospheric surface-layer transport of CO_2 from geologic carbon sequestration sites. Vadose Zone Journal 3:848–857

Oldenburg CM, Lewicki JL, Hepple RP (2003) Near-surface monitoring strategies for geologic carbon dioxide storage verification. Lawrence Berkeley National Laboratory Report LBNL-54089

Oskarsson N (1990) Carbon dioxide bursts of lake Nyos, Cameroon, modeled as a periodic supersaturation in a countercurrent reactor. J Volcanol Geotherm Res 42:307–318

Pellicer, J, Garcia-Morales V, Hernandez MJ (2000) On the demonstration of the Young–Laplace equation in introductory physics courses. Phys Educ 35(2):126–129

Roosevelt SE, Corapcioglu MY (1998) Air bubble migration in a granular porous medium: Experimental studies. Water Resour Res 34(5):1131–1142

Rosenberry DO, Glaser PH, Siegle DI, Weeks EP (2003) Use of hydraulic head to estimate volumetric gas content and ebullition flux in northern peatlands. Water Resour Res 39:1066. DOI 10.1029/2002WR001377

Shipton ZK, Evans JP, Dockrill B, Heath J, Williams A, Kirschner D, Kolesar PT (2004a) Natural leaking CO_2-charged systems as analogs for failed geologic sequestration reservoirs. In: Thomas D, Benson SM (eds) Carbon dioxide capture for storage in deep geologic formations—results from the CO_2 capture project, vol 2. Geologic storage of carbon dioxide with monitoring and verification, Elsevier, Amsterdam

Shipton ZK, Evans JP, Kirschner D, Kolesar PT, Williams AP, Heath J (2004b) Analysis of CO_2 leakage through "low-permeability" faults from natural reservoirs in the Colorado Plateau, east-central Utah. In: Baines SJ, Worden RH (eds) Geological storage of carbon dioxide, vol 233. Geological Society of London, Special Publications, pp 43–58

Sigurdsson H, Devine JD, Tchoua FM, Presser TS, Pringle MKW, Evans WC (1987) Origin of the lethal gas burst from Lake Monoun, Cameroun. J Volcanol Geotherm Res 31:1–16

Smith LK, Lewis WM, Chanton JP, Cronin G, Hamilton SK (2000) Methane emissions from the Orinoco River floodplain, Venezuela. Biogeochemistry 51:113–140

Spycher N, Pruess K (2004) CO_2-H_2O mixtures in the geological sequestration of CO_2. II. Partitioning in chloride brines at 12–100°C and up to 600 bar. Lawrence Berkeley National Laboratory Report LBNL-56334

Spycher N, Ennis-King J, Pruess K (2003) CO_2-H_2O mixtures in the geological sequestration of CO_2. I. Assessment and calculation of mutual solubilities from 12 to 100°C and up to 600 bar. Geochemica et Cosmochimica Acta 67:3015–3031

Torp TA, Gale J (2004) Demonstrating storage of CO_2 in geological reservoirs: The sleipner and SACS projects. Energy 29(9–10):1361–1369

Walter BP, Heimann M (2000) A process-based, climate sensitive model to derive methane emissions from natural wetlands: Application of five wetland sites, sensitivity to model parameters, and climate. Global Biogeochem Cycles 14:745–765

Wan J, Veerapaneni S, Gadelle F, Tokunaga TK (2001) Generation of stable microbubbles and their transport through porous media. Water Resour Res 37(5):1173–1182

Washburn L, Johnson C, Gotschalk CC, Egland ET (2001) A gas-capture buoy for measuring bubbling gas flux in oceans and lakes. J Atm Ocean Technol 18:1411–1420

Wilson JO, Crill PM, Bartlett KB, Sebacher DI, Harriss RC, Sann RL (1989) Seasonal variation of methane emissions from a temperate swamp. Biogeochemistry 8:55–71